BULLETIN OF THE POLISH ACADEMY OF SCIENCES
TECHNICAL SCIENCES, Vol. 68, No. 3, 2020
DOI: 10.24425/bpasts.2020.133124

A study on color vegetation canopy images denoising algorithm

C. WANG[1], Y. LIU[1]*, and P. WANG[2]

[1] College of Information and Computer Engineering, Northeast Forestry University, Harbin 150001, China
[2] College of Mechanical and Electrical Engineering, Northeast Forestry University, Harbin 150001, China

Abstract. Due to the characteristics of color vegetation canopy images which have multiple details and Gaussion noise interference, the adaptive mean filtering (AMF) algorithm is used to perform the denoising experiments on noised images in RGB and YUV color space. Based on the single color characteristics of color vegetation canopy images, a simplified AMF algorithm is proposed in this paper to shorten the overall running time of the denoising algorithm by simplifying the adaptive denoising processing of the component V, which contains less image details. Experimental results show that this method can effectively reduce the running time of the algorithm while maintaining a good denoising effect.

Key words: image denoising, color vegetation canopy images, adaptive mean filtering, color space.

1. Introduction

In application fields such as checking green belt, investigating regional vegetation characteristics and monitoring the growth of experimental forest, color vegetation canopy image is the most important information source. Such images are easily disturbed by natural factors, such as wind and rain, and mixed with image noise, as they are usually collected outdoor or even in the wild. This makes studies on color vegetation canopy image denoising technology particularly important.

In recent years, many scholars have contributed to the study of image denoising technology and achieved good results [1–8]. Paper [1] introduced a new CT image denoising method based on the generative adversarial network (GAN) with Wasserstein distance and perceptual similarity, which yielded a promising clinical result. Paper [2] proposed a fast and flexible denoising convolutional neural network, namely FFDNet, achieving a good trade-off between inference speed and denoising performance. A novel two-stage adaptive framework for denoising of differential interference contrast (DIC) images followed by Gabor based gray-level co-occurrence matrix (GLCM) feature extraction methodology is proposed in paper [3]. In paper [5], an efficient denoising method derived from morphological filtering in nonsubsampled shearlet transform (NSST) domain and Bitonic filtering was proposed. The method achieves reasonable and consistent denoising performance, specifically at high noise levels. Paper [8] proposed a hybrid filtering optimization method of contaminated spot image denoising method to deal with contaminated spots in near-sea-surface images. However, the methods mentioned above are only effective for single-channel grayscale image. The color information is lost once the color image has been processed. In the field of multi-channel filtering, many effective image denoising algorithms have been proposed in recent years [9–18]. In paper [9], Muhammad proposed a norm weighted fusion estimation method based on wavelet domain. The method holds the significant geometric structure of the given noisy image during the denoising process and has a good denoising effect on an image with high level of noise. Linear and nonlinear 2-D image processing approaches are analyzed with the aim of removing the noise from data acquired by distributed optical fiber sensors based on Brillouin optical time-domain analysis (BOTDA) in [11]. The authors also proposed an optimization procedure to find the optimal parameters of the non-local means (NLM) method for BOTDA data denoising. However, when the proposed methods are used to denoise vegetation canopy images, many edge details are lost. The denoising results are below expectations. In [14] effective stacked denoising networks are proposed. The denoising process is decomposed into two stages. Firstly, the noise mapping of the noisy image is predicted, and then the image is denoised to further improve the visual quality and alleviate Gaussian noise overfitting. Paper [15] proposed a 2-D finite-impulse response (FIR) Wiener filter driven by the adaptive cuckoo search (ACS) algorithm for denoising multispectral satellite images contaminated with the Gaussian noise of different variance levels. The ACS algorithm was proposed to optimize the Wiener weights for obtaining the best possible estimate of the desired uncorrupted image. The stability and convergence of the algorithm were analyzed, and the possibility of its application in the field of satellite images analysis was proved. To address the fact that different bands of hyperspectral images have different noise levels, HSI denoising method, taking into account the band relationship and different noise levels, was proposed in paper [17]. According to the characteristics of the target noise bands, this method selects some related but quality superior bands, and then fuses the selected related bands to realize the denoise of the target noise bands. These methods can well retain the edge details of the image, but the algorithms are complex and the processing speed is slow.

*e-mail: smith@university.edu.pl

Manuscript submitted 2019-04-13, revised 2019-09-06, initially accepted for publication 2019-09-11, published in June 2020

As objects of processing, color vegetation canopy images, have very prominent characteristics. They are easy to be mixed with Gaussian noise, have complex edge details, and the main color of the images is usually yellow-green. According to the above characteristics, this paper proposes a simplified adaptive mean filtering (AMF) algorithm for YUV color space, in order to remove Gaussian noise effectively while retaining the edge details and improving the operation speed.

The main contributions of this paper can be summarized as:

- The processing range of the AMF algorithm is extended to multi-channel color images.
- According to the characteristics of vegetation canopy images which have single color, transforming the image into YUV color space before denoising allows for eliminating the adaptive processing of component V and improving the overall operation speed of the algorithm.

The rest of the paper is organized as follows. In Section 2, adaptive mean filtering (AMF) algorithm used to remove the Gaussian noise is introduced. In Section 3 color space RGB and YUV and their conversion relations are considered. In Section 4 experimental results of color vegetation canopy images denoising are shown. In Section 5, the evaluation index of denoising effect is calculated and the experimental results are analyzed. Conclusions are drawn in Section 6.

2. Adaptive mean filtering (AMF) algorithm

The most classical algorithms of image denoising are median filtering and mean filtering. The denoising principle of these two algorithms is to change the pixel value of all the points in the box (the set of the target pixel and its surrounding pixels) into their median value or mean value, so as to achieve the effect of noise smoothing. However, there is an obvious defect in these processing methods. The algorithms treat all the pixels in the image equally, without considering the uniform part, the edge and texture, and the differences in the human eyes' sensitivity to different parts of the image. The defect makes the processed images lose a substantial amount of edge and detail information. Especially when the images with complex edges and details are processed, such as vegetation canopy images, the results are always severely distorted. In contrast, the adaptive image filtering algorithm can distinguish the useless noise signal and the useful edge and texture information in the image independently. The algorithm preserves the edge, texture and other details of the image while removing the noise. In this way, the problems of distortion and blurring are largely avoided [19–22].

Consider $f(x, y)$ is the image to be processed. Under the effect of the degradation function $h(x, y)$ and the noise signal $n(x, y)$, the image $f(x, y)$ is degraded to $g(x, y)$, which is an image mixed with noise. In the time domain, the process of image degradation can be expressed as:

$$g(x, y) = h(x, y) * f(x, y) + n(x, y), \tag{1}$$

In the frequency domain, it can be expressed as:

$$G(u, v) = H(u, v)F(u, v) + N(u, v), \tag{2}$$

where $G(u, v)$, $H(u, v)$, $F(u, v)$, $N(u, v)$ are the Fourier transform of $g(x, y)$, $h(x, y)$, $f(x, y)$, $n(x, y)$.

When only the denoising algorithm is studied, the degradation equation can be simplified as:

$$g(x, y) = f(x, y) + n(x, y). \tag{3}$$

Given $g(x, y)$ and some information about $h(x, y)$ and $n(x, y)$, the process of image denoising is equivalent to the estimate calculation of the image $f(x, y)$. Let us define the estimated value of $f(x, y)$ as $\hat{f}(x, y)$. The diagram of the degenerate-restore process is shown in Fig. 1.

The noise in the vegetation canopy images mainly comes from the interference of natural outdoor conditions, and its main component is Gaussian noise. So the mean filter which has better Gaussian noise removal effect is selected to combine with the adaptive method for the image denoising. The formula can be expressed as follows:

$$\begin{aligned} \hat{f}(x, y) &= g(x, y) - \hat{n}(x, y) = \\ &= g(x, y) - \frac{\sigma_g^2}{\hat{\sigma}_L^2}\left[g(x, y) - \hat{\mu}_L\right], \end{aligned} \tag{4}$$

where $\hat{n}(x, y)$ is the estimated value of the noise, σ_g^2 is the noise variance of $g(x, y)$, $\hat{\sigma}_L^2$ is the gray variance of pixel values

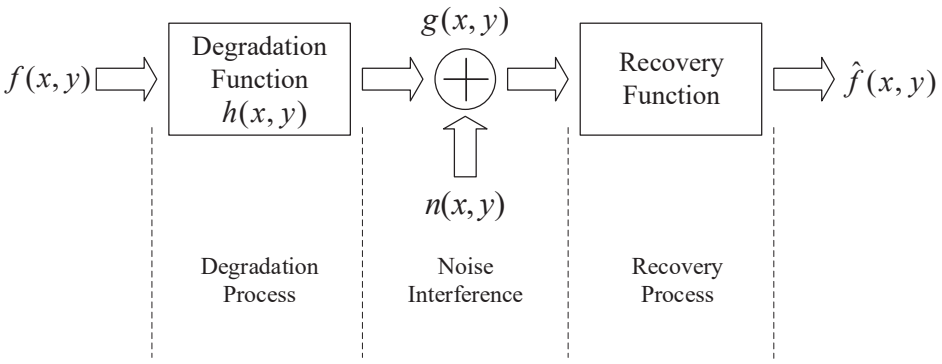

Fig. 1. The diagram of the degenerate-restore process

around point (x, y) (in the Box), and $\hat{\mu}_L$ is the gray average of pixel values around point (x, y) (in the box).

The computation results of (4) will vary with the relationship between σ_g^2 and $\hat{\sigma}_L^2$:

- If $\sigma_g^2 = 0$, there is no noise interference. Thus, (4) can be written as $\hat{f}(x, y) = g(x, y)$, and the algorithm does not perform any image processing.
- If $\hat{\sigma}_L^2 \gg \sigma_g^2$, the variance of the pixels in the box is much greater than the noise variance of $g(x, y)$, which means that the box contains image details such as edges and textures. Thus, (4) can be written as $\hat{f}(x, y) = g(x, y)$, and the detail information of the image is preserved.
- If $\hat{\sigma}_L^2 \approx \sigma_g^2$, the variance of the pixels in the box is similar to the noise variance of $g(x, y)$, which means that the image region in the box is uniform. Thus, (4) can be written as $\hat{f}(x, y) = \hat{\mu}_L$, and mean filtering is used for denoising the box.

The logic flowchart of AMF is shown in Fig. 2.

3. RGB and YUV color spaces

Color space is an abstract mathematical model that uses a group of color components (usually three or four) to express different

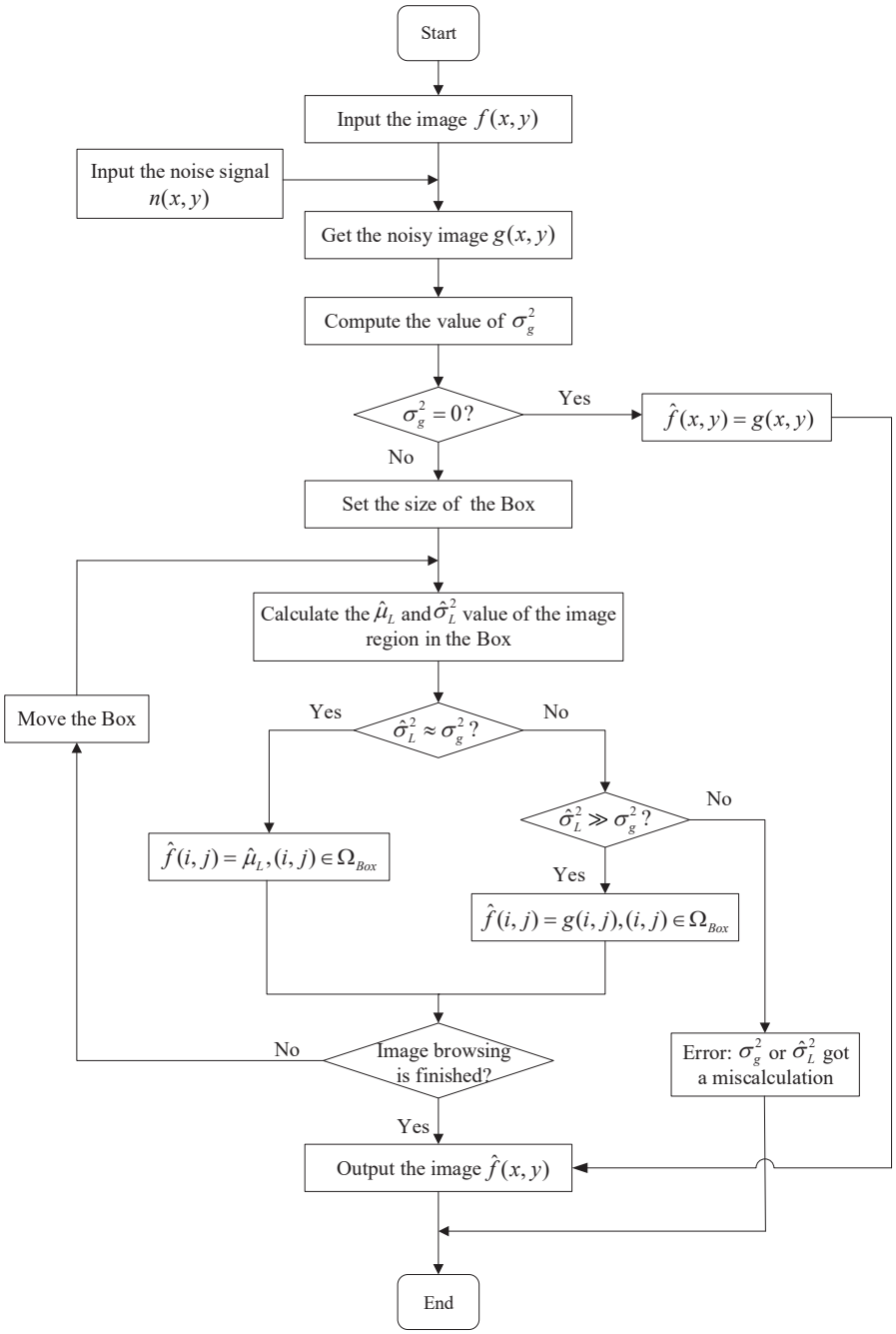

Fig. 2. The flowchart of the adaptive mean filtering (AMF) algorithm

colors in a certain dimensional coordinate. The common color spaces are RGB, CMYK, HSV, YUV, YIQ, Lab, etc. Different color spaces have different expression range and expression rules, which are suitable for color image processing in different conditions. For example, CMYK is usually used for color printing, HSV for computer graphics, and YIQ for color TV systems. In this paper, considering the characteristics of color vegetation canopy images, only RGB and YUV color space are discussed in detail.

3.1. RGB color space. RGB color space is the most classic and commonly used color space, especially for CRT display, video, multimedia and web design. The core design principle of RGB is that any color light in nature can be mixed by red, green and blue light in different proportions. Therefore, it can express almost all the colors that can be recognized by human eyes.

The greatest advantage of RGB color space is that the principle is simple and intuitive – very easy to understand. But it also has obvious disadvantages. The three components R, G and B are highly correlated. If one of the components changes, the mixed color will also change a lot. So the integration of the three components always results in errors, after the three components are processed separately. In addition, due to the inherent physiological characteristics of the human eye, the sensitivity to changes in luminance and chrominance is not the same, and the sensitivity to red, green, blue color components is not the same either. Therefore, the visual uniformity of RGB color space is poor, and the visual color difference before the two colors cannot be equivalent to the distance between the two points in the color space.

3.2. YUV color space. Some early studies show that human eye is more sensitive to luminance information than to chrominance information [23]. Therefore, to a certain extent, the compression of chrominance information will not affect the visual effect of the human eye. Based on the above conclusion, YUV color space separates luminance information from chrominance information.

In the color space, component Y is used to represent the luminance information of the image, that is, the grayscale value. Also, human eye has different sensitivity to the brightness of red, green and blue color components [24–26].

Components U and V are used to represent the chrominance of the image, that is, to describe the color and saturation of the image. They are obtained by compressing R, G and B components in different proportions. The U component represents the chromatism from yellow green to bluish violet. The V component represents the chromatism from cyan to magenta. The relationship between the two components is shown in Fig. 3.

The transformation between YUV color space and RGB color space can be achieved by a simple matrix operation:

$$\begin{cases} Y = 0.299\times R + 0.587\times G + 0.114\times B \\ U = -0.147\times R - 0.289\times G + 0.436\times B \\ V = 0.615\times R - 0.515\times G - 0.100\times B \end{cases}, \tag{5}$$

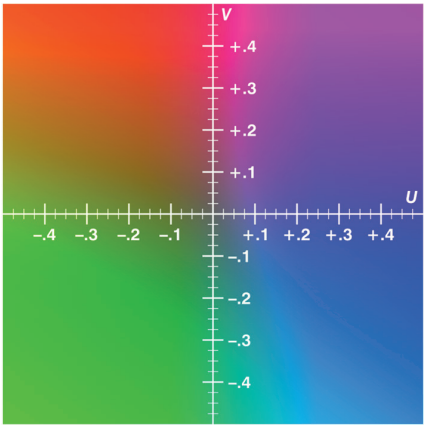

Fig. 3. The relationship between the U and V components

$$\begin{cases} R = Y + 1.140\times V \\ G = Y - 0.394\times U - 0.581\times V \\ B = Y + 2.032U \end{cases}, \tag{6}$$

The YUV color space has a smaller amount of data than RGB for the same color image, which leads to faster processing speed and lower algorithm complexity. The relative independence between the luminance component Y and the chrominance components U and V also reduces the possible image distortion in the process of components compounding, after processing each component separately.

As for the color vegetation canopy image, its main tone is yellow-green. The main chrominance information of the image is concentrated in the component U, and the component V contains very little information about the image chrominance details. Therefore, when denoising this kind of images, the detail processing of component V can be simplified, which will greatly improve the efficiency of the algorithm.

4. Denoising experiment on color vegetation canopy images

In this paper, 20 color canopy images are used for denoising experiments with the size of 1200×1200 pixels and the representation form is fractional real values. 6 of them were selected to show as samples in Fig. 4. The selected images have vegetation features as green trees, yellow trees, dead trees, low shrubs, grasslands and plant shadows, which are representative.

In order to simulate the natural noise signal, the images were mixed with Gaussian noise (the average value is 0.1 and the variance is 0.01). The images with Gaussian noise are shown in Fig. 5.

Since the default reading format of the image is established in the RGB color space, the first experiment consists in denoising the noisy images in RGB. The AMF denoising results of the three components are shown in Fig. 6. The denoised color images of the 6 image samples, obtained by integrating the three components are shown in Fig. 7.

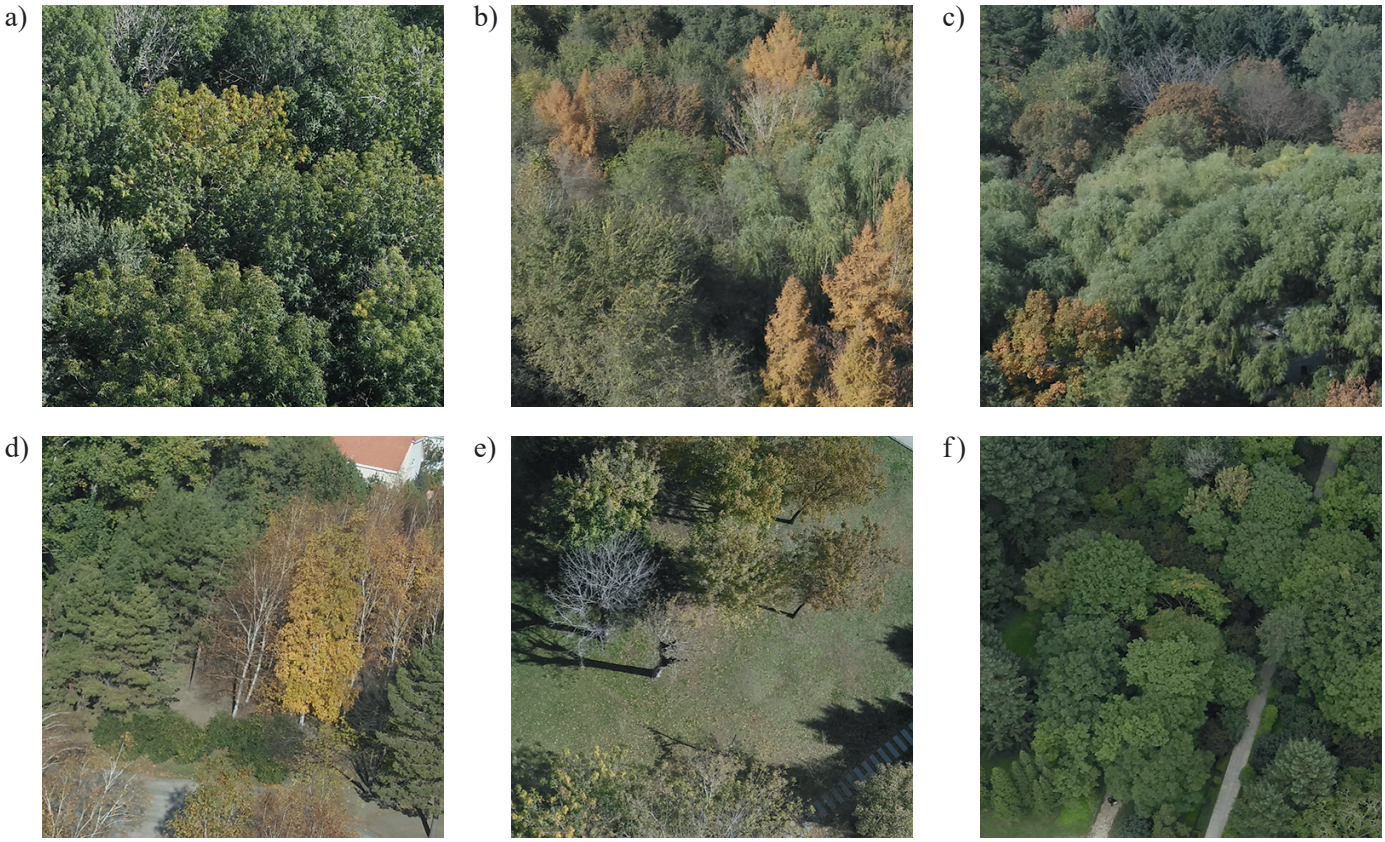

Fig. 4. Original color vegetation canopy image samples

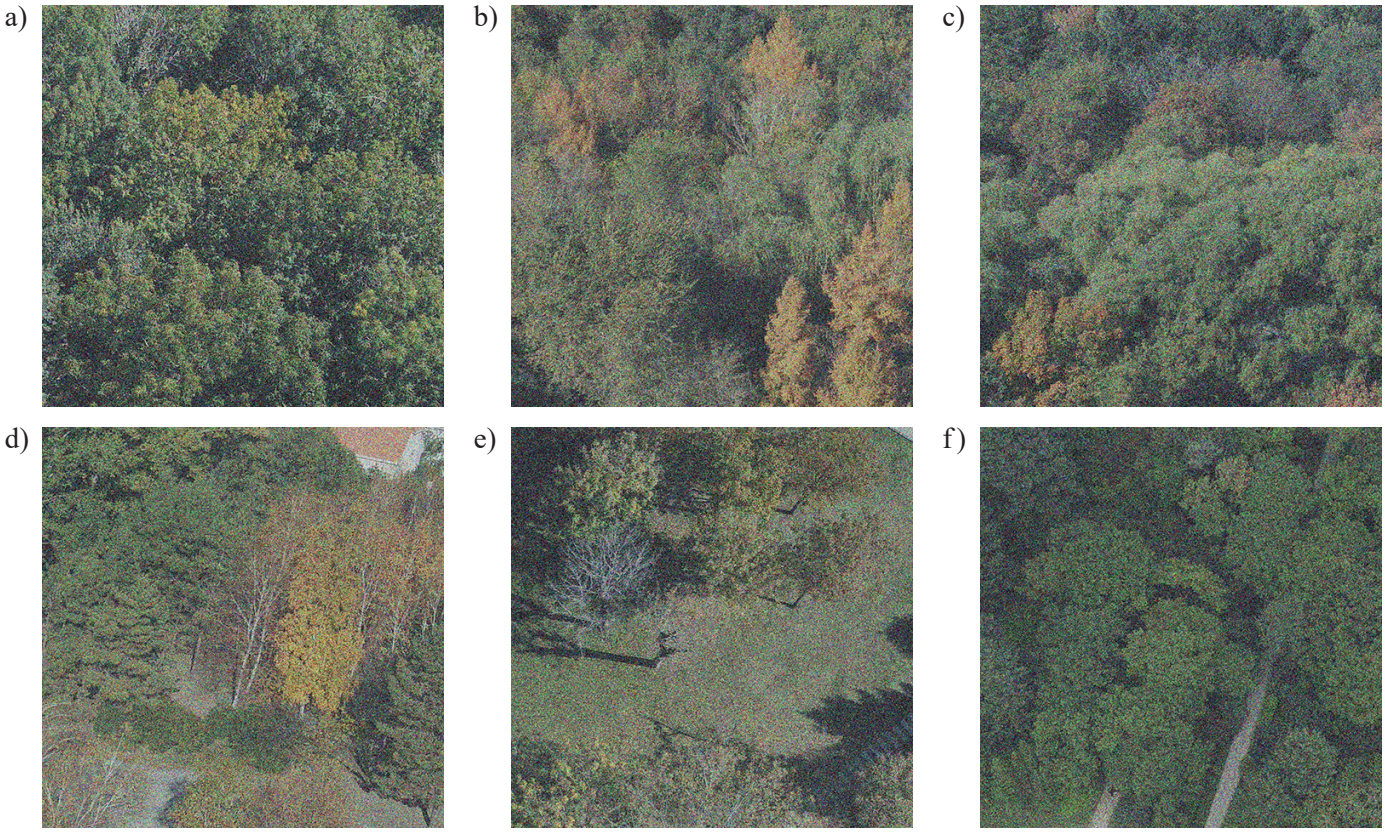

Fig. 5. Color vegetation canopy image mixed with Gaussian noise (the average value is 0.1 and the variance is 0.01)

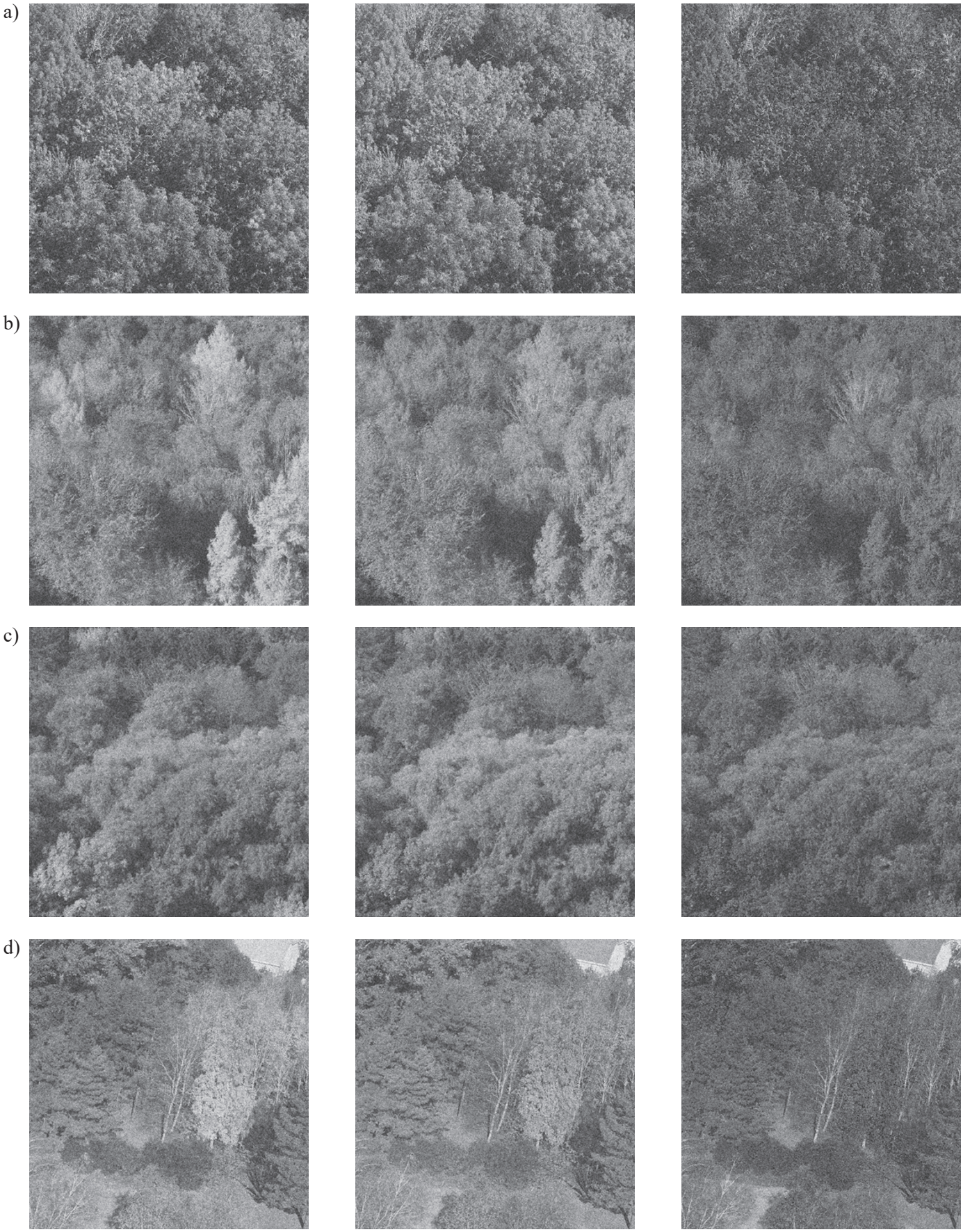

Fig. 6. The AMF denoising results of the R, G, B components of the images in Fig. 5 (components R, G and B are shown from left to right)

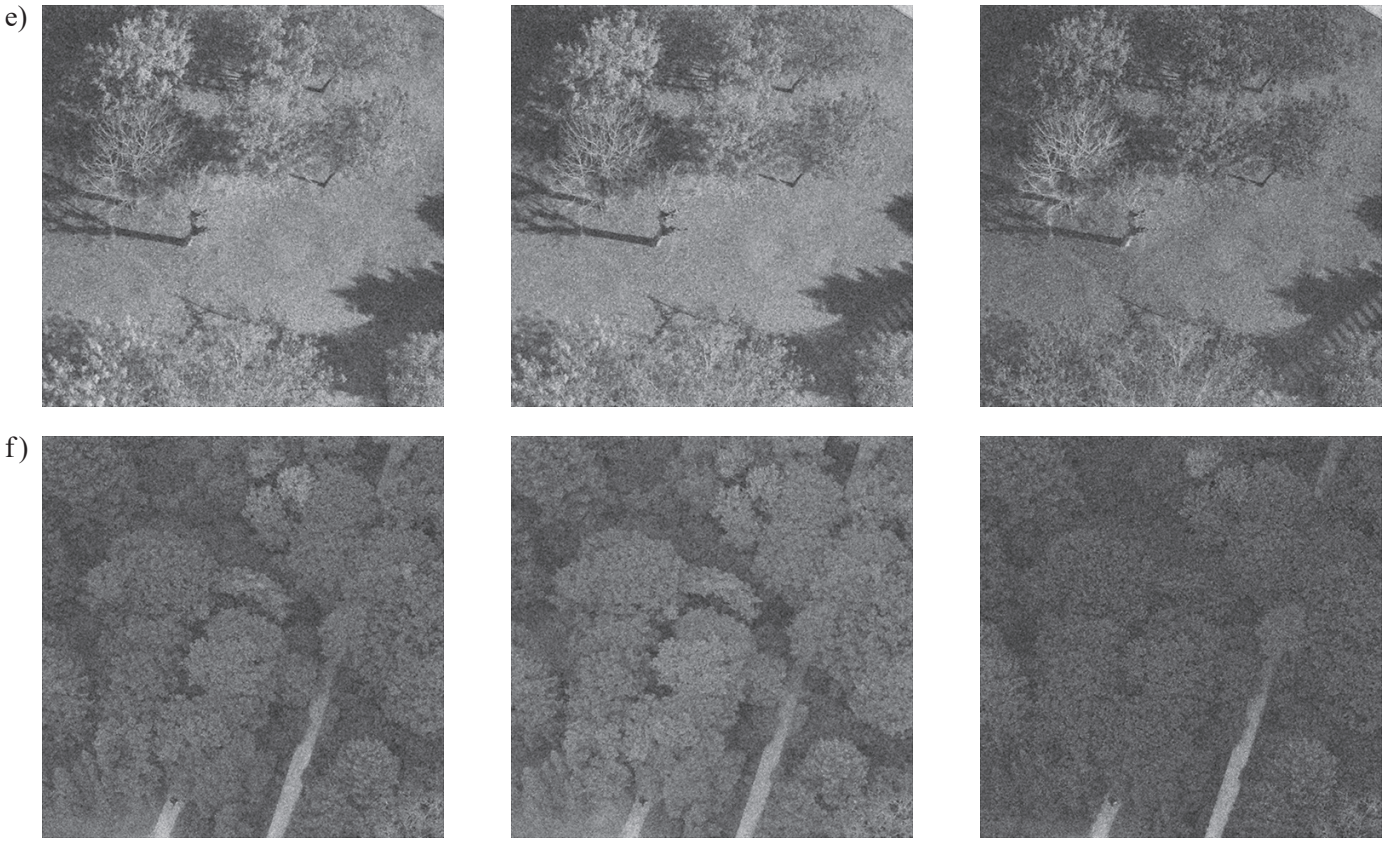

Fig. 6. The AMF denoising results of the R, G, B components of the images in Fig. 5 (components R, G and B are shown from left to right)

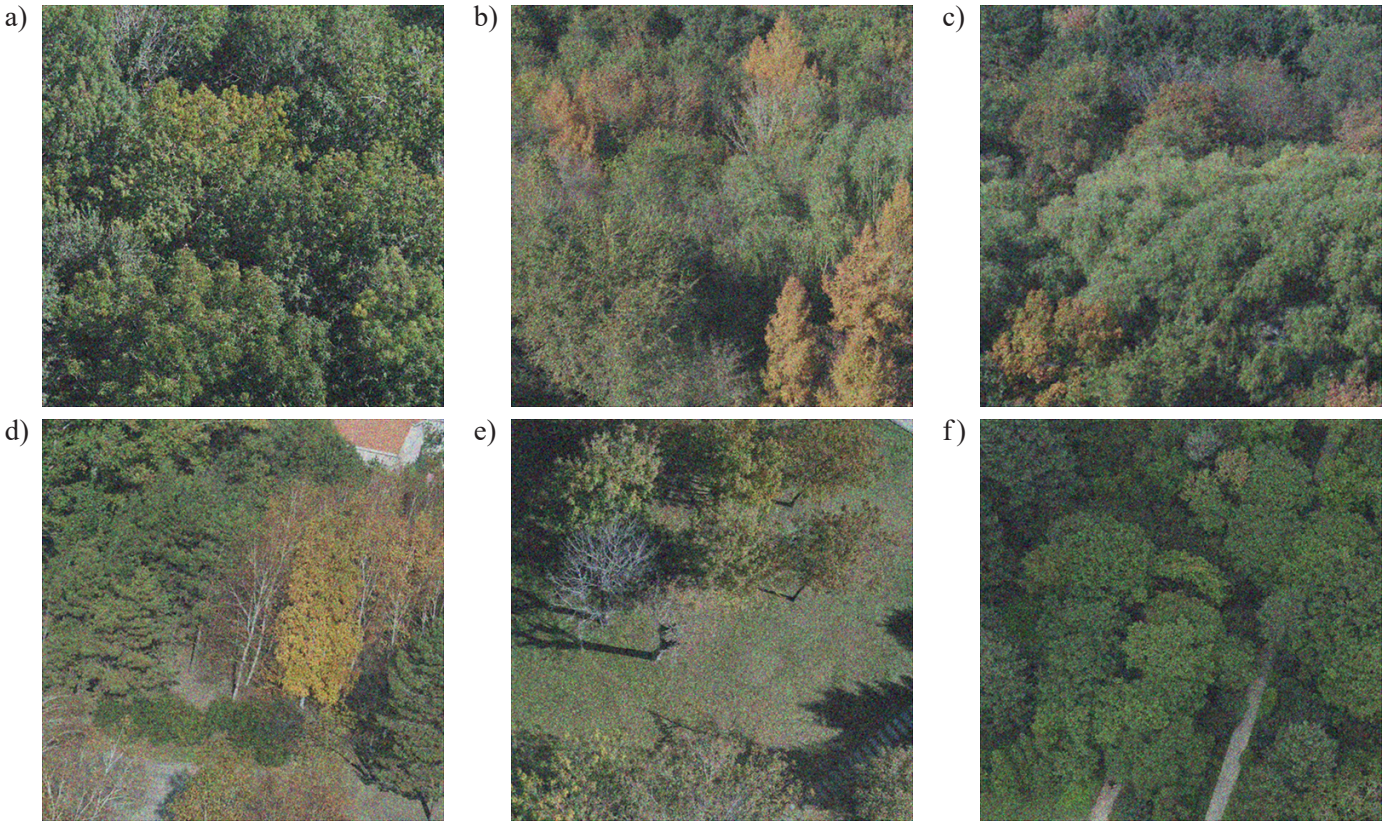

Fig. 7. AMF denoising results in color space RGB of the images in Fig. 5

The noisy images in Fig. 5 are transformed into color space YUV. The Y, U and V components are denoised by AMF, and the denoised component images and color images are shown in Fig. 8 and Fig. 9, respectively.

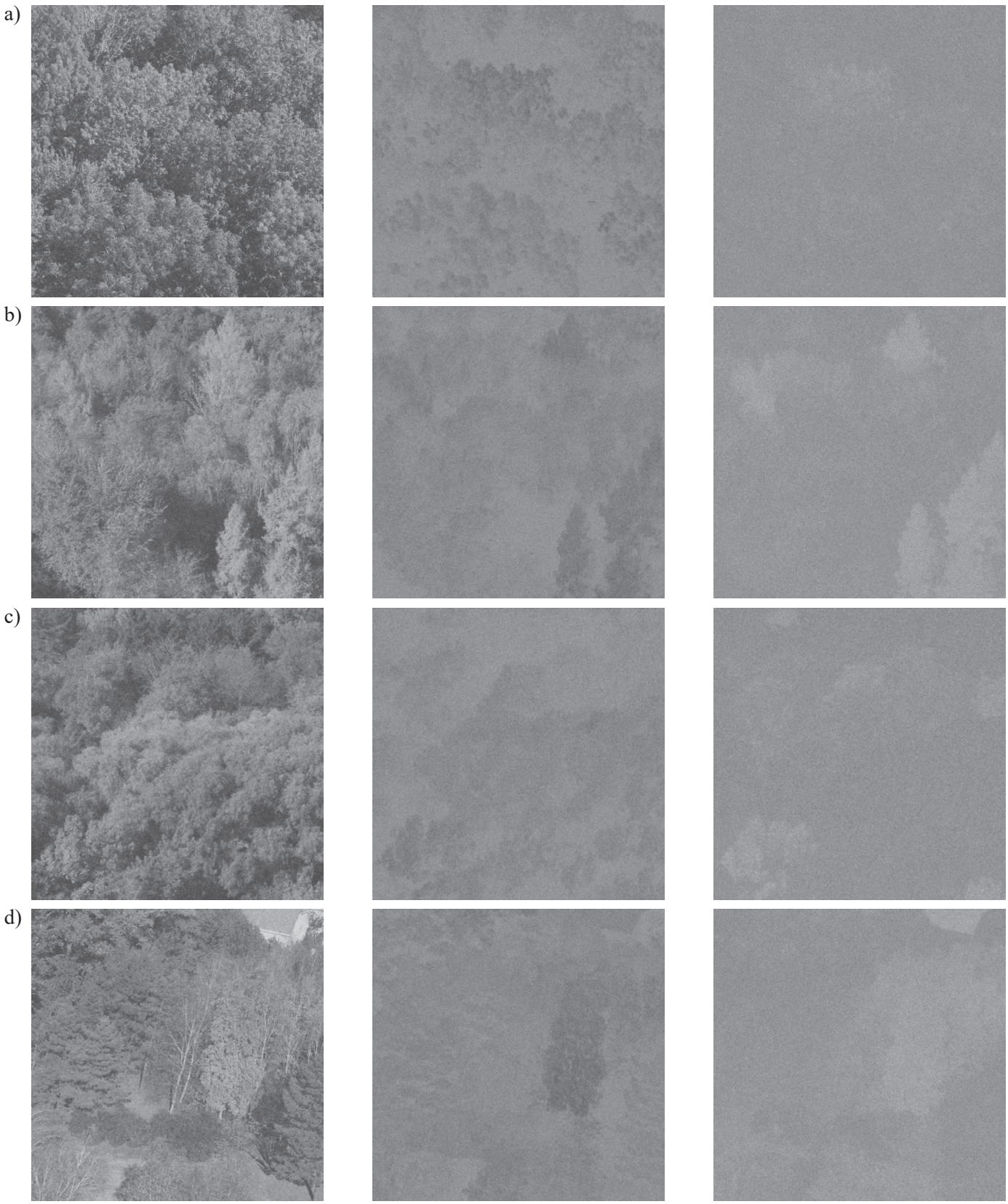

Fig. 8. AMF denoising results of the Y, U, V components of the images in Fig. 5 (components Y, U and V are shown from left to right)

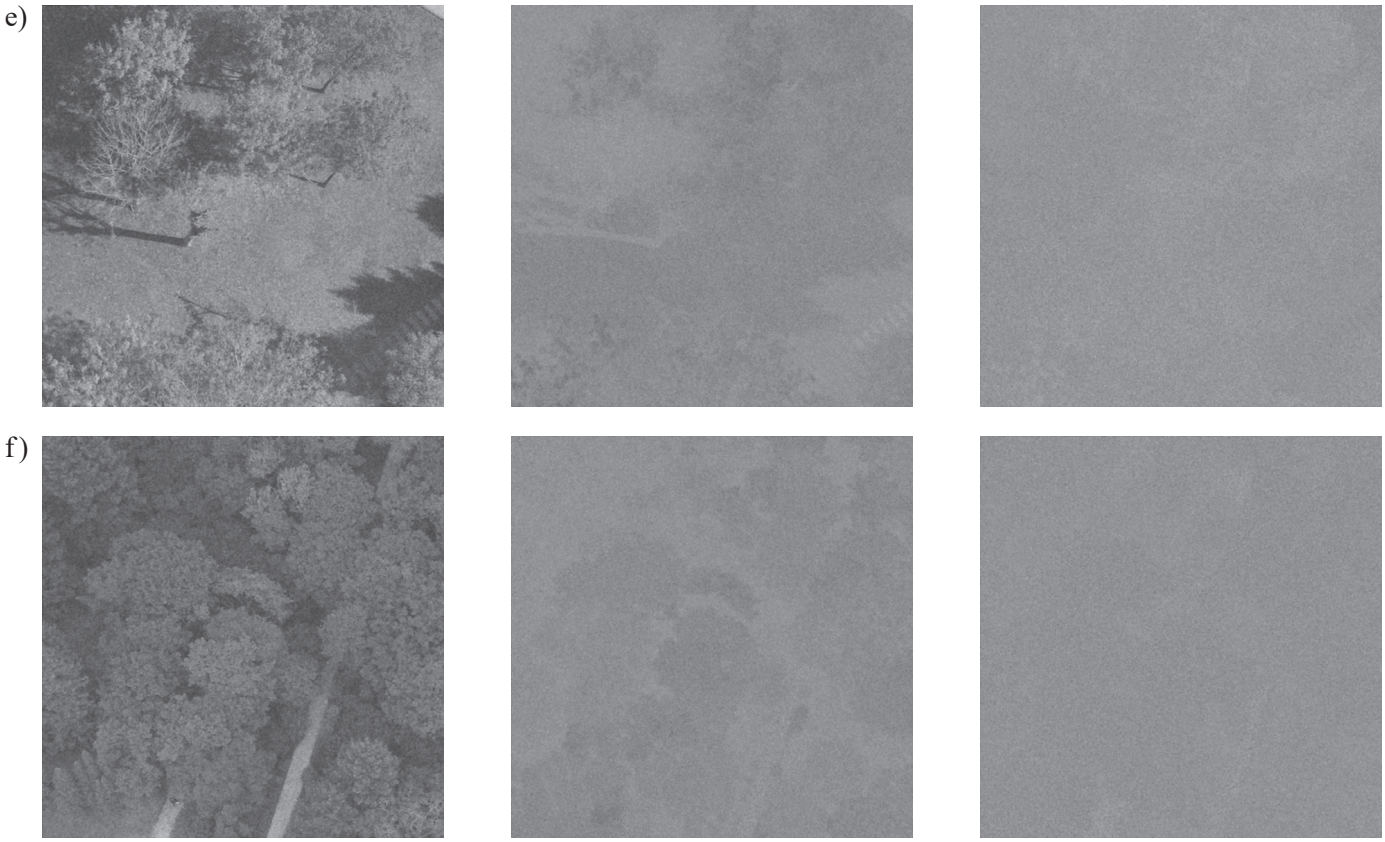

Fig. 8. AMF denoising results of the Y, U, V components of the images in Fig. 5 (components Y, U and V are shown from left to right)

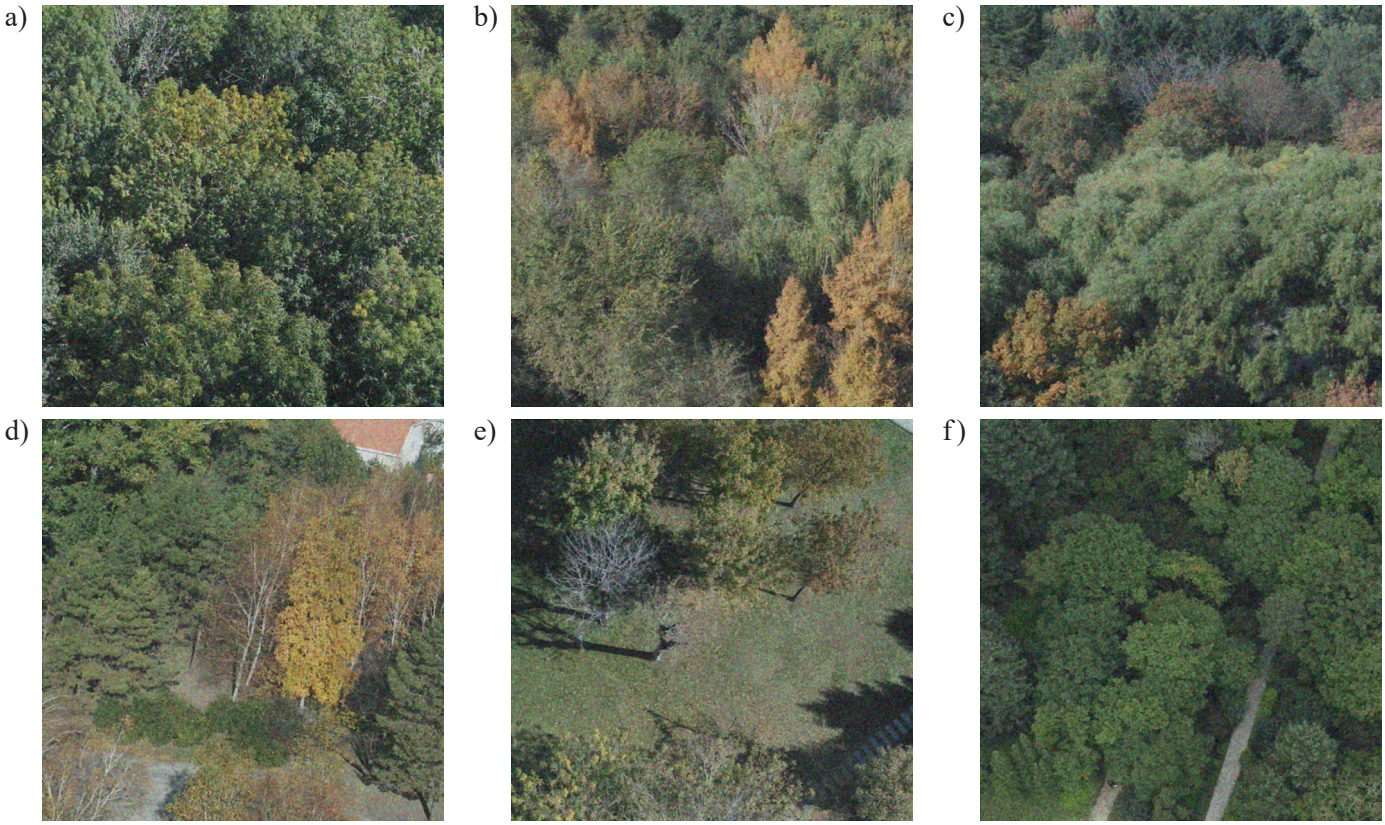

Fig. 9. AMF denoising results in color space YUV of the images in Fig. 5

It can be seen in Fig. 6 that the three image components in the RGB color space all contain much image detail information. Fig. 8 shows that, in the YUV color space, the image details are mainly reflected in the component Y, a small amount in the component U, while the details contained in the component V are very few. Therefore, to denoising the component V by original mean filtering instead of AMF is attempted.

The denoised images of the component V are shown in Fig. 10. Combine the denoised component V with the components Y and U in Fig. 8 to obtain the color images. The color vegetation canopy images denoised by the simplified algorithm are shown in Fig. 11.

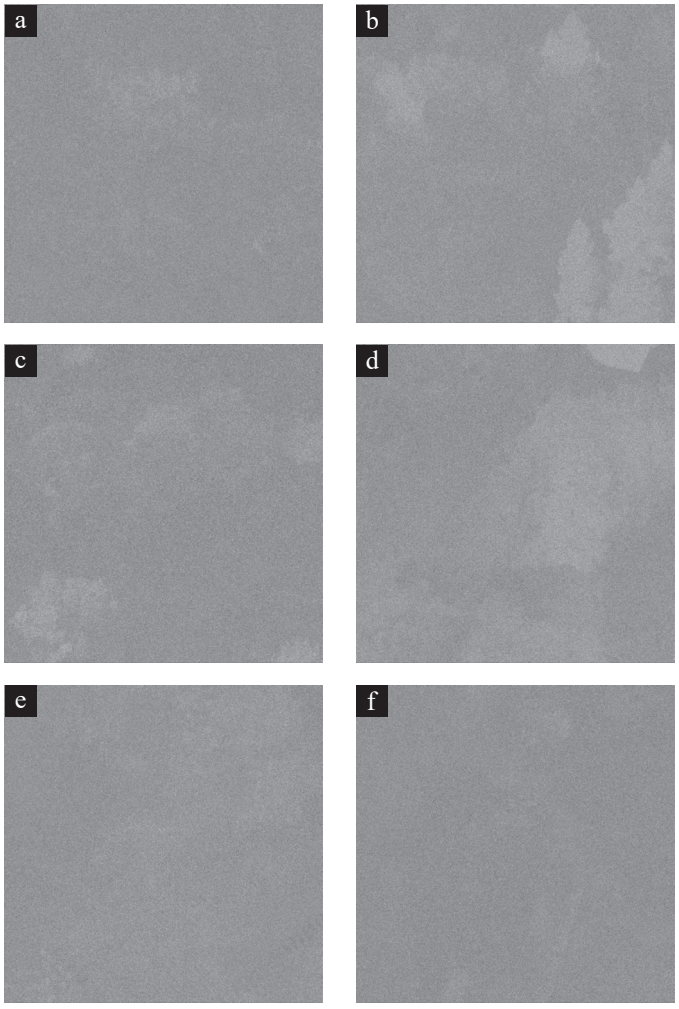

Fig. 10. The V components denoised by original mean filtering

The average running times of the three denoising methods for all experimental images (a–t) are listed in Table 1.

In order to better prove the effectiveness of the method proposed in this paper, the experimental images are mixed with Gaussian noise with mean value of 0.1 and variance of 0.1. The image samples are shown in Fig. 12.

The denoising experimental results of AMF in color space RGB for the noisy images in Fig. 12 are shown in

Table 1
The average running time of the three denoising methods for all experimental images (mixed with Gaussian noise with average value of 0.1 and variance of 0.01)

Time (s)	AMF in RGB	AMF in YUV	Simplified AMF in YUV
Image a	0.41	0.47	0.32
Image b	0.37	0.47	0.30
Image c	0.30	0.44	0.27
Image d	0.39	0.46	0.29
Image e	0.38	0.46	0.33
Image f	0.35	0.45	0.31
……	……	……	……
Image p	0.34	0.43	0.29
Image q	0.39	0.48	0.30
Image r	0.42	0.49	0.34
Image s	0.40	0.48	0.33
Image t	0.33	0.39	0.26

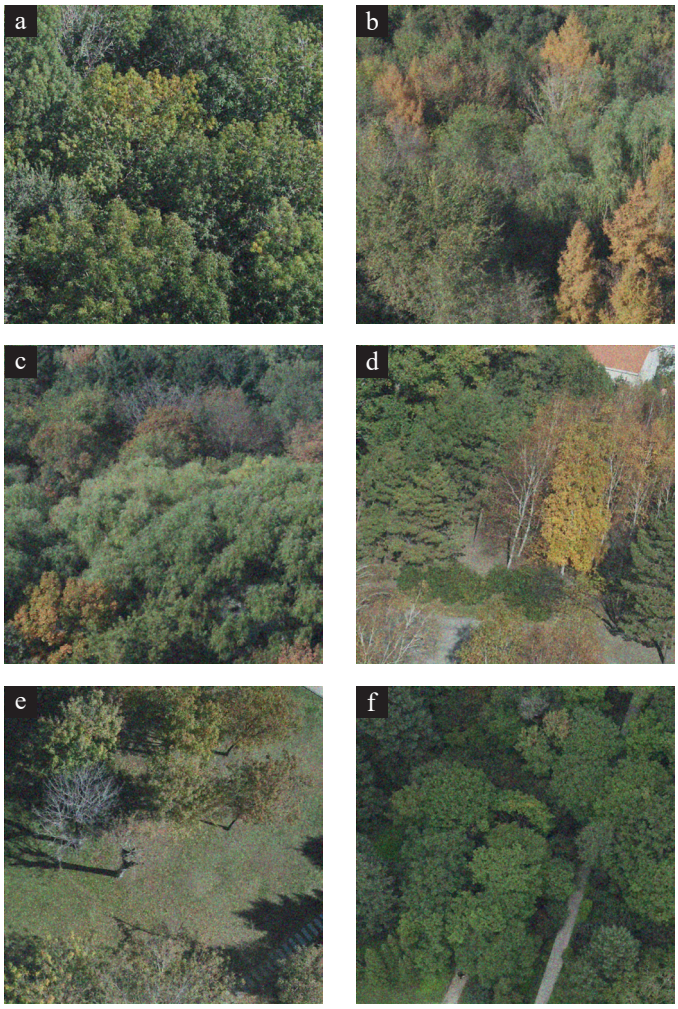

Fig. 11. The simplified AMF denoising results in color space YUV of the images in Fig. 5

Fig. 12. The color vegetation canopy image mixed with Gaussian noise (the average value is 0.1 and the variance is 0.1)

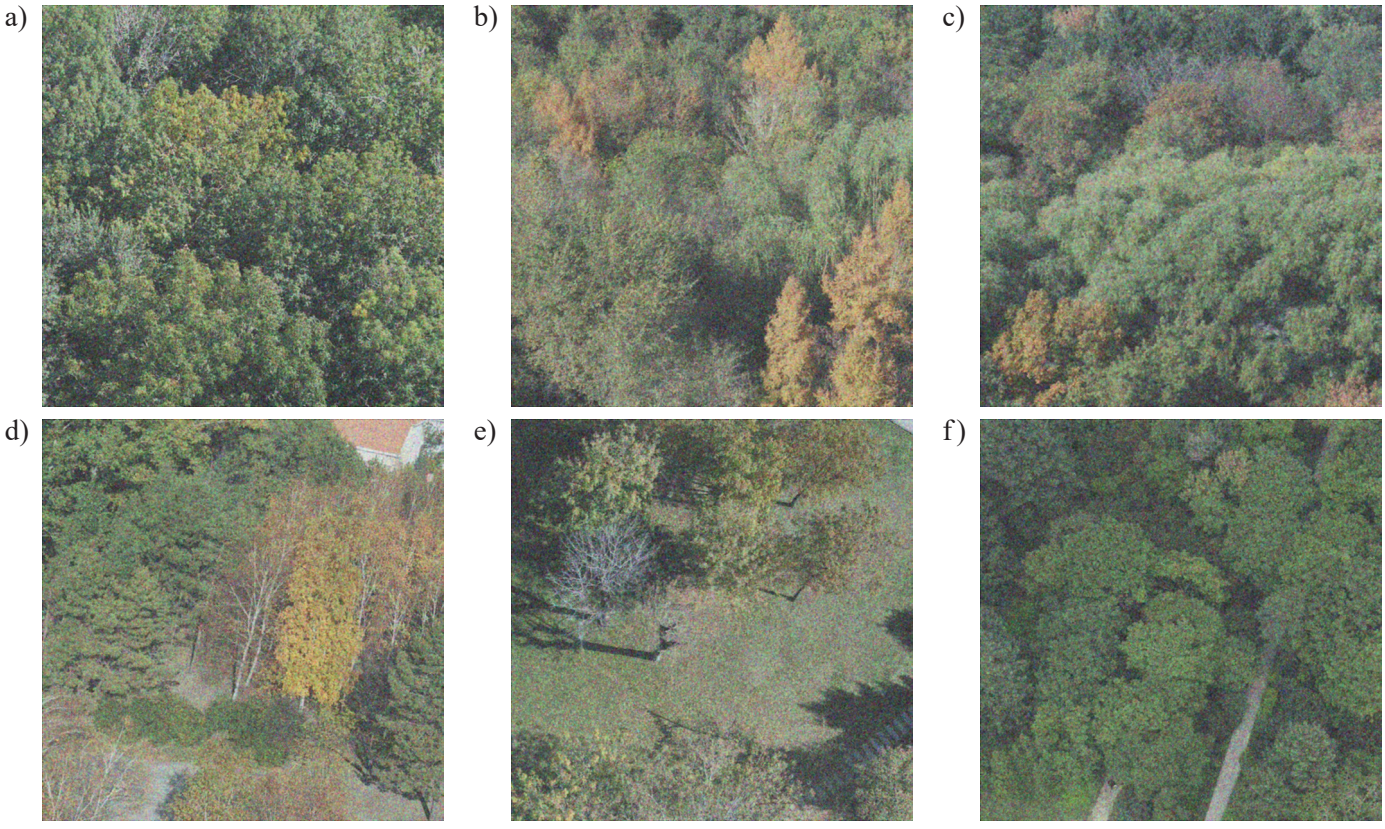

Fig. 13. AMF denoising results in color space RGB of the images in Fig. 12

Fig. 13. The denoising experimental results of AMF in color space YUV are shown in Fig. 14, and the denoising experimental results of simplified AMF in color space YUV are shown in Fig. 15.

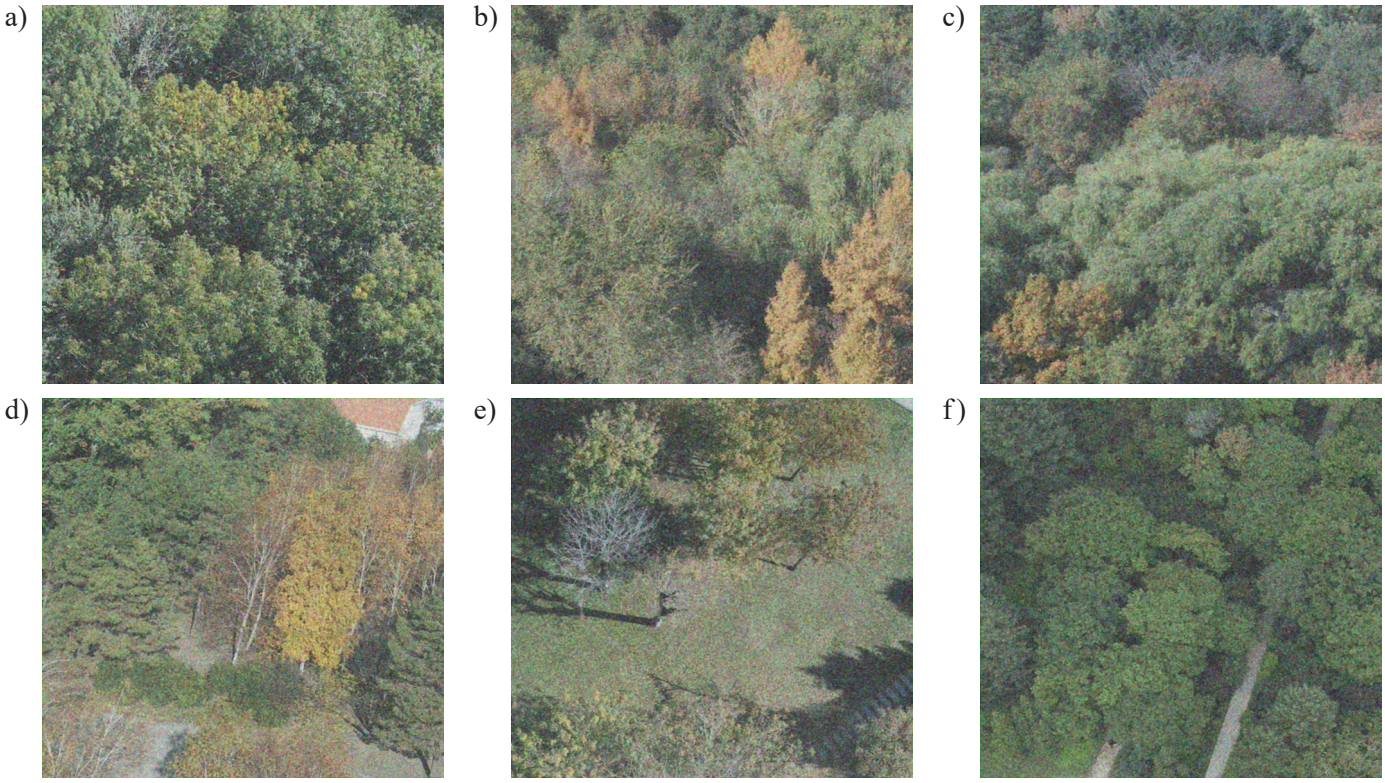

Fig. 14. AMF denoising results in color space YUV of the images in Fig. 12

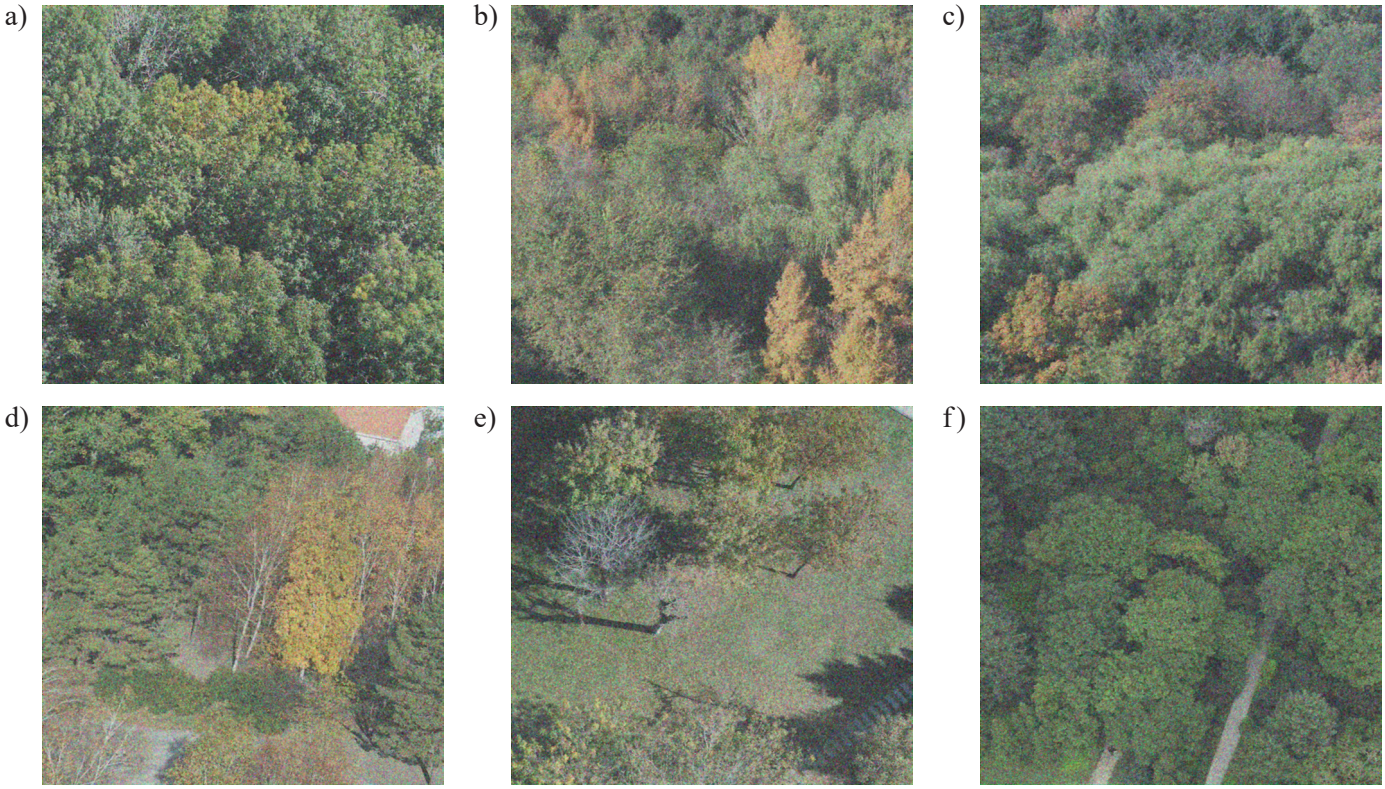

Fig. 15. The simplified AMF denoising results in color space YUV of the images in Fig. 12

Table 2
The average running time of the three denoising methods for all experimental images (mixed with Gaussian noise of average value 0.1 and variance 0.1)

Time (s)	AMF in RGB	AMF in YUV	Simplified AMF in YUV
Image a	0.44	0.48	0.36
Image b	0.40	0.44	0.33
Image c	0.32	0.43	0.30
Image d	0.37	0.43	0.32
Image e	0.41	0.45	0.33
Image f	0.39	0.43	0.33

Time (s)	AMF in RGB	AMF in YUV	Simplified AMF in YUV
……	……	……	……
Image p	0.39	0.46	0.31
Image q	0.33	0.46	0.30
Image r	0.43	0.45	0.33
Image s	0.40	0.49	0.34
Image t	0.34	0.39	0.28

The average running time of the three denoising methods for all experimental images (a–t) are listed in Table 2.

Further, Gaussian noise with mean value of 0 and variance of 0.1 is mixed into the experimental images. The image samples are shown in Fig. 16.

The denoising experimental results of AMF in color space RGB for the noisy images in Fig. 16 are shown in Fig. 17. The denoising experimental results of AMF in color space YUV are shown in Fig. 18. The denoising experimental results of simplified AMF in color space YUV are shown in Fig. 19.

Fig. 16. The color vegetation canopy image mixed with Gaussian noise (the average value is 0 and the variance is 0.1)

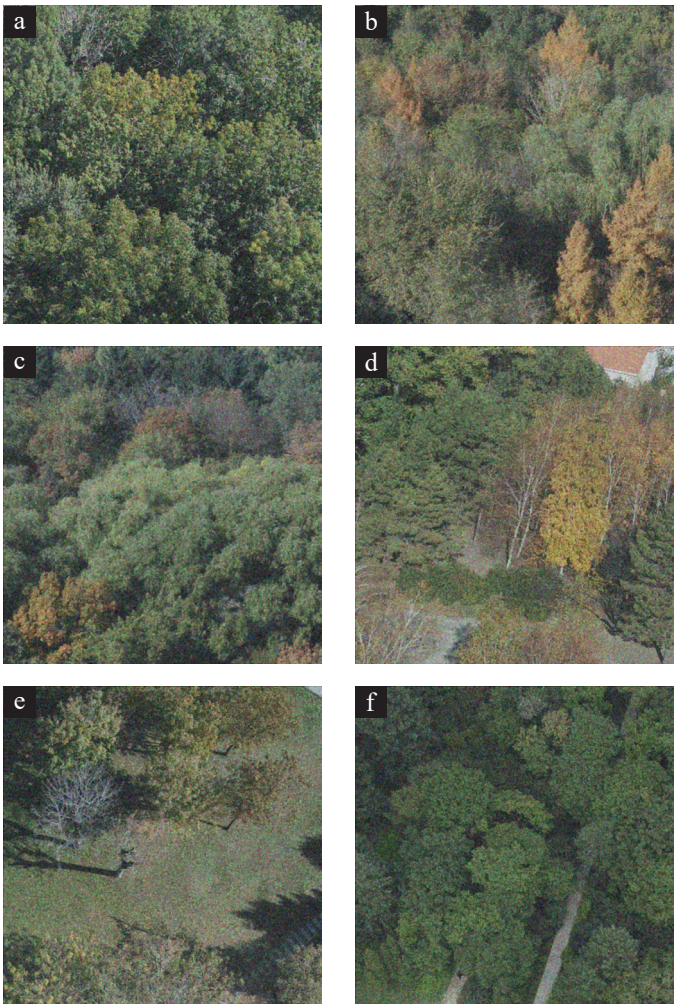

Fig. 17. AMF denoising results in color space RGB of the images in Fig. 16

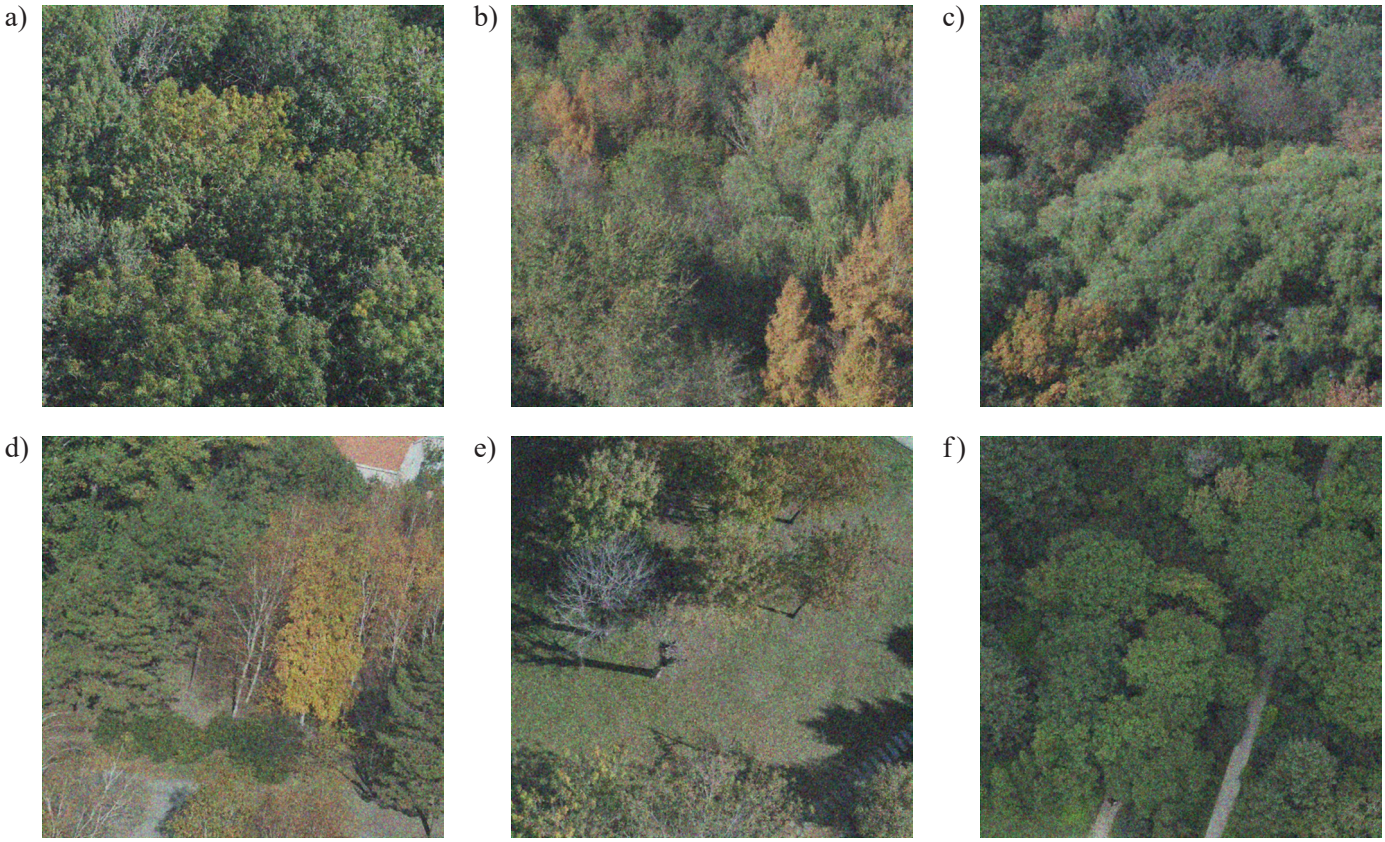

Fig. 18. AMF denoising results in color space YUV of the images in Fig. 16

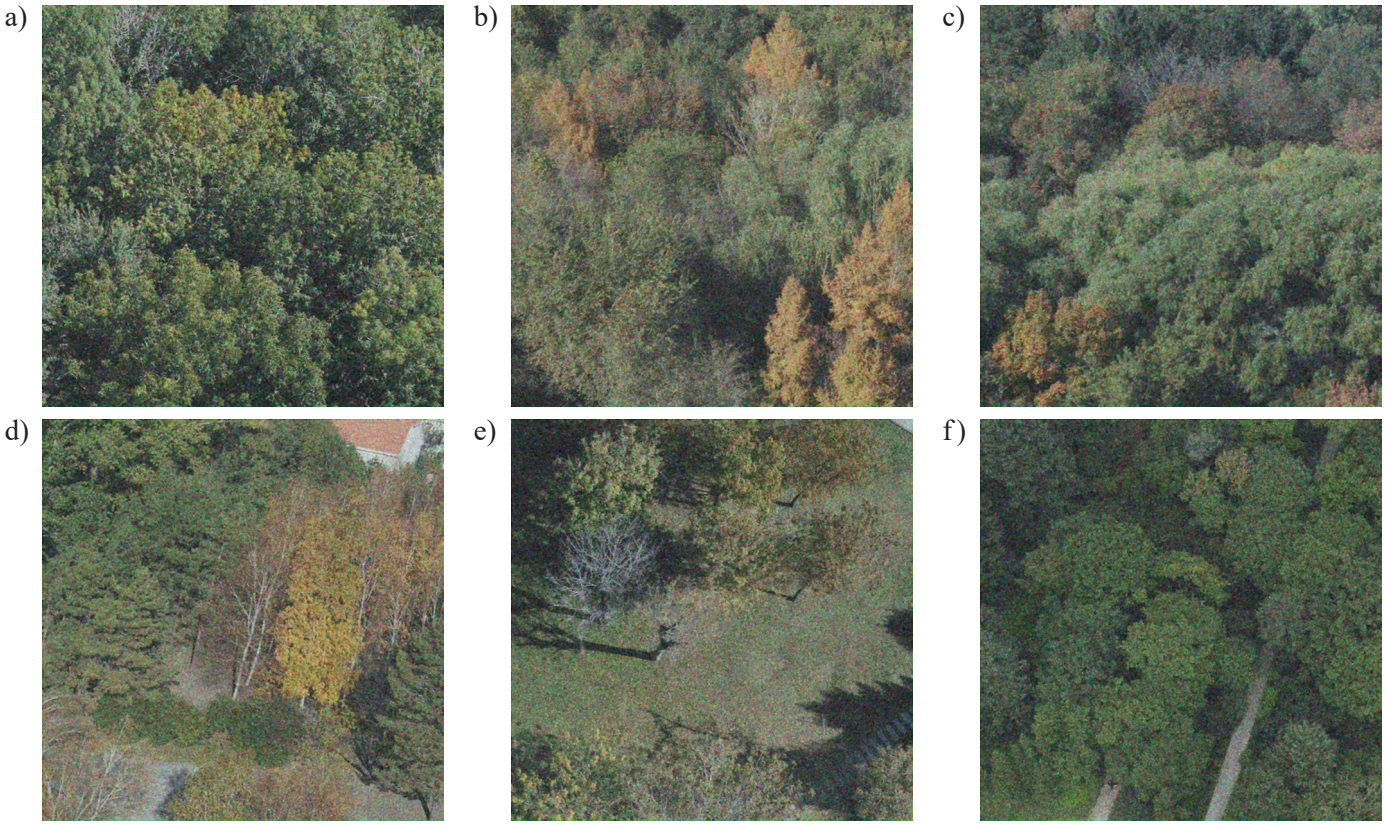

Fig. 19. Simplified AMF denoising results in color space YUV of the images in Fig. 16

The average running time of the three denoising methods for all experimental images (a–t) are listed in Table 3.

Table 3
The average running time of the three denoising methods for all experimental images (mixed with Gaussian noise with average value 0 and variance 0.1)

Time (s)	AMF in RGB	AMF in YUV	Simplified AMF in YUV	Time (s)	AMF in RGB	AMF in YUV	Simplified AMF in YUV
Image a	0.38	0.43	0.31	**……**	……	……	……
Image b	0.39	0.46	0.32	**Image p**	0.40	0.46	0.32
Image c	0.35	0.42	0.30	**Image q**	0.33	0.43	0.27
Image d	0.33	0.40	0.26	**Image r**	0.44	0.50	0.35
Image e	0.38	0.46	0.31	**Image s**	0.45	0.49	0.34
Image f	0.39	0.45	0.30	**Image t**	0.39	0.44	0.28

5. Calculation of image quality evaluation parameters and analysis

5.1. Calculation of PNSR (peak signal to noise ratio). PNSR is the ratio of the peak signal power to the destructive noise power [27]. It can be calculated according to the following equation:

$$PSNR = 10 \cdot \log_{10}\left(\frac{MAX^2}{MSE}\right), \tag{7}$$

where MAX is the maximum value of pixels in the image, generally 255. MSE is the mean square error. For two monochrome images I and K with the same size of $m \times n$, MSE can be expressed as:

$$MSE = \frac{1}{mn}\sum_{i=0}^{m-1}\sum_{j=0}^{n-1}\left[I(\mathrm{i},\mathrm{j}) - \mathrm{K}(\mathrm{i},\mathrm{j})\right]^2, \tag{8}$$

As for color images in RGB and YUV color space, since each pixel point has three component values, MSE can be expressed as:

$$MSE = \frac{1}{3mn}\sum_{i=0}^{m-1}\sum_{j=0}^{n-1}\sum_{k=0}^{2}\left[I(\mathrm{i},\mathrm{j},\mathrm{k}) - \mathrm{K}(\mathrm{i},\mathrm{j},\mathrm{k})\right]^2, \tag{9}$$

The PNSR values of the original color vegetation canopy images (a–t) and their denoised images processed by the three denoising algorithms are calculated, and the results are listed in Tables 4–6.

Table 4
PNSR of the original color vegetation canopy images and the denoised images (mixed with Gaussian noise which average value is 0.1 and variance is 0.01)

PNSR	PNSR of images (a–t)		
	AMF in RGB	AMF in YUV	Simplified AMF in YUV
Image a	20.0584	21.5898	21.4389
Image b	22.9513	24.9004	24.5428
Image c	23.1949	25.4588	25.0533
Image d	22.7502	24.6003	24.2651
Image e	22.2215	24.1669	23.8962
Image f	23.0521	26.0038	25.6264
……	……	……	……
Image p	23.2842	23.9234	23.3285
Image q	21.4986	22.2374	22.0234
Image r	22.5389	24.3945	23.7882
Image s	22.2485	23.2457	22.3597
Image t	23.2398	24.9342	24.1469

Table 5
PNSR of the original color vegetation canopy images and the denoised images (mixed with Gaussian noise which average value is 0.1 and variance is 0.1)

PNSR	PNSR of images (a–t)		
	AMF in RGB	AMF in YUV	Simplified AMF in YUV
Image a	21.3135	22.3021	22.2123
Image b	22.9834	24.4573	24.4477
Image c	24.5659	25.8943	25.7813
Image d	22.8324	24.6235	24.2333
Image e	23.3554	24.4673	24.3465
Image f	22.5658	24.7826	24.6635
……	……	……	……
Image p	23.4452	23.5345	23.5262
Image q	20.9340	22.3823	22.1225
Image r	21.7843	24.2345	23.1491
Image s	23.4395	24.8261	23.7323
Image t	22.0485	24.5773	24.4239

Table 6
PNSR of the original color vegetation canopy images and the denoised images (mixed with Gaussian noise which average value is 0 and variance is 0.1)

PNSR	PNSR of images (a–t)		
	AMF in RGB	AMF in YUV	Simplified AMF in YUV
Image a	20.4563	21.8636	21.7257
Image b	22.2549	23.4502	23.3974
Image c	22.0138	24.1856	24.1056
Image d	22.4783	23.4587	23.3977
Image e	21.2984	22.4621	22.3458
Image f	21.9223	23.7345	23.6345
.....	.....	.....	.....
Image p	23.3459	24.8436	24.8014
Image q	23.4986	25.0457	24.9245
Image r	22.8561	24.7837	23.6954
Image s	22.5465	23.8256	23.7256
Image t	21.3788	22.7524	22.7245

5.2. Calculation of FSIM (feature similarity). The human eye has different sensitivity to different pixels in the image. For example, the pixels at the position of edges and intersections are more likely to attract the attention of human eye. Compared with PNSR, FSIM takes this feature into consideration and takes it as the basis for evaluating image quality [28].

To calculate the FSIM value of two images, it is necessary to calculate the phase consistency similarity and the gradient magnitude similarity:

$$S_{PC} = \frac{2PC_1 \cdot PC_2 + T_1}{PC_1^2 + PC_2^2 + T_1}, \tag{10}$$

$$S_{GM} = \frac{2GM_1 \cdot GM_2 + T_2}{GM_1^2 + GM_2^2 + T_2}, \tag{11}$$

where, PC_1 and PC_2 are the PC (phase congruency) values of the two images, which reflect the image information of structure, edge and texture [29]. GM_1 and GM_2 are the GM (gradient magnitude) values, which reflect the image information of brightness and contrast [30]. T_1 and T_2 are constants, and their function is to avoid the systematic error that occurs when the denominator is 0.

By combining (10) and (11), the comprehensive similarity of the two images can be expressed as:

$$S_L = {S_{PC}}^{\alpha} \cdot {S_{GM}}^{\beta}, \tag{12}$$

where, α and β are the weight coefficients, generally 1.

If a pixel x has high PC values in the two images, it indicates that this pixel has a high influence in the similarity evaluation of the two images based on human visual characteristics (HVS). Therefore, FSIM can be expressed as follows:

$$FSIM = \frac{\sum_{x \in \Omega} S_L(\mathrm{x}) \cdot \mathrm{PC}_m(\mathrm{x})}{\sum_{x \in \Omega} PC_m(\mathrm{x})}, \tag{13}$$

where, $PC_m(\mathrm{x}) = \max[PC_1(\mathrm{x}), \mathrm{PC}_2(\mathrm{x})]$, and Ω represents the entire region of the image.

When comparing two color images, (13) can be written as:

$$FSIM = \frac{\sum_{x \in \Omega} S_L(\mathrm{x}) \cdot [S_C(\mathrm{x})]^{\lambda} \cdot \mathrm{PC}_m(\mathrm{x})}{\sum_{x \in \Omega} PC_m(\mathrm{x})}, \tag{14}$$

where, S_C is the chrominance similarity of the two images, which is obtained by calculating the image components containing chrominance information according to the similarity formula. λ is the weight coefficient.

FSIM values of the original color vegetation canopy images (a–t) and their denoised images processed by the three denoising algorithms are calculated, and the results are listed in Tables 7–9.

Table 7
FSIM of the original color vegetation canopy images and the denoised images (mixed with Gaussian noise with average value of 0.1 and variance of 0.01)

FSIM	FSIM of images (a–t)		
	AMF in RGB	AMF in YUV	Simplified AMF in YUV
Image a	0.9320	0.9600	0.9579
Image b	0.9237	0.9538	0.9520
Image c	0.9025	0.9369	0.9357
Image d	0.9235	0.9532	0.9518
Image e	0.9200	0.9516	0.9511
Image f	0.9074	0.9425	0.9410
.....	.....	.....	.....
Image p	0.9238	0.9503	0.9497
Image q	0.9347	0.9589	0.9574
Image r	0.9096	0.9322	0.9315
Image s	0.9394	0.9579	0.9550
Image t	0.9168	0.9428	0.9421

Table 8
FSIM of the original color vegetation canopy images and the denoised images (mixed with Gaussian noise with average value of 0.1 and variance of 0.1)

FSIM	FSIM of images (a–t)		
	AMF in RGB	AMF in YUV	Simplified AMF in YUV
Image a	0.9239	0.9673	0.9535
Image b	0.9045	0.9398	0.9325
Image c	0.9134	0.9424	0.9399
Image d	0.9392	0.9561	0.9514
Image e	0.9235	0.9503	0.9486
Image f	0.9382	0.9579	0.9551
.....	.....	.....	.....
Image p	0.9037	0.9403	0.9389
Image q	0.9187	0.9486	0.9443
Image r	0.9375	0.9535	0.9501
Image s	0.9331	0.9584	0.9573
Image t	0.9284	0.9496	0.9475

Table 9
FSIM of the original color vegetation canopy images and the denoised images (mixed with Gaussian noise with average value of 0 and variance of 0.1)

FSIM	FSIM of images (a–t)		
	AMF in RGB	AMF in YUV	Simplified AMF in YUV
Image a	0.9183	0.9397	0.9359
Image b	0.9042	0.9489	0.9452
Image c	0.9273	0.9582	0.9553
Image d	0.9274	0.9501	0.9482
Image e	0.9136	0.9398	0.9371
Image f	0.9252	0.9482	0.9463
.....	.....	.....	.....
Image p	0.9317	0.9582	0.9560
Image q	0.9023	0.9402	0.9381
Image r	0.9264	0.9493	0.9479
Image s	0.9291	0.9498	0.9478
Image t	0.9174	0.9532	0.9498

5.3. Analysis of the experimental results. It can be seen from Tables 1–3, Tables 4–6 and Tables 7–9 that, for color vegetation canopy images, the AMF denoising effect in YUV color space is better than that in RGB color space. However, because of the color space conversion, the running time of the AMF denoising algorithm in YUV space is relatively prolonged. After the simplification of the denoising process of component V, the running time of the denoising algorithm in YUV space is greatly reduced, and the good denoising effect is maintained at the same time.

6. Conclusions

In this paper, AMF algorithm was adopted to denoise the color vegetation canopy images. Based on the fact that the images have many details, easy to be mixed with Gaussian noise and have single color, denoising experiments were carried out in RGB and YUV color spaces. It was found in the experiments that the denoising effect in YUV was better than that in RGB color space, due to the low correlation of the three image components in YUV color space. In addition, among the three image components in YUV, V component mainly reflects the chromatism of cyan-magenta in the image. For the color vegetation canopy image with yellow-green as the dominant color, the details contained in V component are very few. Therefore, this paper proposed a simplified AMF algorithm that only used original mean filtering to denoise V component. Experimental results show that this method can effectively reduce the running time of the denoising algorithm while maintaining a good denoising effect. Especially when a large amount of images needs to be processed, it will have good application value.

The method proposed in this paper can be extended to processing of other color images with a single tone feature and has certain follow-up research value.

Acknowledgements. This research was funded by NATIONAL NATURAL SCIENCE FOUNDATION OF CHINA (Number: 31370565).

References

[1] Q. Yang, P. Yan, Y. Zhang, H. Yu, Y. Shi, X. Mou, and G. Wang, "Low-dose CT image denoising using a generative adversarial network with Wasserstein distance and perceptual loss", *IEEE Trans. Med. Imaging* 37(6), 1348–1357 (2018).

[2] K. Zhang, W. Zuo, and L. Zhang, "FFDNet: Toward a fast and flexible solution for CNN-based image denoising", *IEEE Trans. Image Process* 27(9), 4608–4622 (2018).

[3] S. Mukhopadhyay, S. Pratiher, S. Mukherjee, D. Dasgupta, N. Ghosh, and P. K. Panigrahi, "A two-stage framework for DIC image denoising and Gabor based GLCM feature extraction for pre-cancer diagnosis", *High-Speed Biomedical Imaging and Spectroscopy III: Toward Big Data Instrumentation and Management* 10505, 1050512 (2018).

[4] A. Kumar, M.O. Ahmad, and M.N.S. Swamy, "Tchebichef and Adaptive Steerable Based Total Variation Model for Image Denoising", *IEEE Trans. Image Process* 28(6), 2921–2035 (2019).

[5] B. Goyal, A. Dogra, S. Agrawal, and B.S. Sohi, "Two-dimensional gray scale image denoising via morphological operations in NSST domain & bitonic filtering", *Future Gener. Comput. Syst.* 82, 158–175 (2018).

[6] H.M. Ali, "MRI medical image denoising by fundamental filters", *High-Resolution Neuroimaging-Basic Physical Principles and Clinical Applications*, Intech, 11–124 (2018).

[7] H. Dawood, M. Iqbal, M. Azhar, H. Ahmad, H. Dawood, Z. Mehmood, and J.S. Alowibdi, "Texture-preserving denoising method for the removal of random-valued impulse noise in gray-scale images", *Opt. Eng.* 58(2), 023103 (2019).

[8] W. Zhu, E. Wang, Y. Hou, L. Xian, and M.A. Ashraf, "Hybrid Filtering Optimization Method for Denoising Contaminated Spot Images at Near-Sea-Surface Intervals", *Journal of Coastal Research* 82, 70–76 (2018).

[9] N. Muhammad, N. Bibi, A. Jahangir, and Z. Mahmood, "Image denoising with norm weighted fusion estimators", *Pattern Analysis and Applications* 21(4), 1013–1022 (2018).

[10] B. Du, Z. Huang, N. Wang, Y. Zhang, and X. Jia, „Joint weighted nuclear norm and total variation regularization for hyperspectral image denoising", *Int. J. Remote Sens.* 39(2), 334–355 (2018).

[11] M.A. Soto, J.A. Ramírez, and L. Thévenaz, "Optimizing Image Denoising for Long-Range Brillouin Distributed Fiber Sensing", *J. Lightwave Technol.* 36(4), 1168–1177 (2018)

[12] A. Stankiewicz, T. Marciniak, A. Dąbrowski, M. Stopa, P. Rakowicz, and E. Marciniak, "Denoising methods for improving automatic segmentation in OCT images of human eye", *Bul. Pol. Ac.: Tech.* 65(1), 71–78 (2017).

[13] H. Wang, Y. Cen, Z. He, R. Zhao, and F. Zhang, "Reweighted low-rank matrix analysis with structural smoothness for image denoising", *IEEE Trans. Image Process.* 27(4), 1777–1892 (2018).

[14] S. Wu, T. Fan, C. Dong, and Y. Qiao, "RDS-Denoiser: a Detail-preserving Convolutional Neural Network for Image Denoising", *2018 IEEE International Conference on Cyborg and Bionic Systems (CBS)*, 127–132 (2018).

[15] S. Suresh, S. Lal, C. Chen, and T. Celik, "Multispectral Satellite Image Denoising via Adaptive Cuckoo Search-Based Wiener Filter", *IEEE Trans. Geosci. Remote Sens.* 56(8), 4334–4345 (2018).

[16] Y.R. Fan, T.Z. Huang, X.L. Zhao, L.J. Deng, and S. Fan, "Multispectral Image Denoising via Nonlocal Multitask Sparse Learning", *Remote Sens.* 10(1), 116 (2018).

[17] X. Zheng, Y. Yuan, and X. Lu, "Hyperspectral Image Denoising by Fusing the Selected Related Bands", *IEEE Trans. Geosci. Remote Sens.* 57(5), 2596–2609 (2018).

[18] H.R. Shahdoosti and S.M. Hazavei, "Combined ripplet and total variation image denoising methods using twin support vector machines", *Multimedia Tools and Applications* 77(6), 7013–7031 (2018).

[19] L. Fan, X. Li, Q. Guo, and C. Zhang, "Nonlocal image denoising using edge-based similarity metric and adaptive parameter selection" *Science China Information Sciences* 61(4), 049101 (2018).

[20] G.C. Goodwin and K.S. Sin, "Adaptive filtering prediction and control Prentice-Hall information and system sciences series", *Prentice-Hall* (1984)

[21] R. Phillip, "Adaptive IIR filtering in signal processing and control" *Routledge*, 2018.

[22] H.D. Nguyen, S.H. Yoo, M.R. Bhutta, and K.S. Hong, "Adaptive filtering of physiological noises in fNIRS data" *Biomed. Eng. Online.* 17(1), 180 (2018).

[23] P.G.J. Baeten, "Contrast sensitivity of the human eye and its effects on image quality", *Technische Universiteitndhoven*, (1999).

[24] D.G. Green, "The contrast sensitivity of the colour mechanisms of the human eye" *The Journal of physiology* 196(2), 415–429 (1968).

[25] R.E. Wrolstad and D.E. Smith, "Color analysis" *Food analysis. Springer*, Boston, MA, 573–586(2010).

[26] K.T. Mullen, "The contrast sensitivity of human colour vision to red-green and blue-yellow chromatic gratings", *The Journal of physiology* 359(1), 381–400 (1985).

[27] J.F. de Boer, B. Cense, B.H. Park, M.C. Pierce, G.J. Tearney, and B.E. Bouma, "Improved signal-to-noise ratio in spectral-domain compared with time-domain optical coherence tomography", *Opt. Lett*. 28(21), 2067–2069 (2003).

[28] L. Zhang, X. Mou, and D. Zhang, "FSIM: A feature similarity index for image quality assessment", *IEEE Trans. Image Process.* 20(8), 2378–2386 (2011).

[29] K. Peter, "Phase congruency: A low-level image invariant", *Psychological research* 64(2), 136–148 (2000).

[30] W. Xue, L. Zhang, X. Mou, and A. C. Bovik, "Gradient magnitude similarity deviation: A highly efficient perceptual image quality index", *IEEE Trans. Image Process.* 23(2), 684–695 (2014).